Annu. Rev. Nucl. Part. Sci. 2001. 51:189–217

PARITY-VIOLATING ELECTRON SCATTERING AND NUCLEON STRUCTURE

D. H. Beck
Department of Physics, University of Illinois at Urbana-Champaign, Urbana, Illinois 61801; e-mail: dhbeck@uiuc.edu

R. D. McKeown
W. K. Kellogg Radiation Laboratory, California Institute of Technology, Pasadena, California 91125; e-mail: bmck@krl.caltech.edu

Key Words parity violation, nucleon form factors, strange form factors, anapole moment, electron scattering

■ **Abstract** The measurement of parity violation in the helicity dependence of electron-nucleon scattering provides unique information about the basic quark structure of the nucleons. This review presents the general formalism of parity-violating electron scattering, with emphasis on elastic electron-nucleon scattering. The physics issues addressed by such experiments are discussed, and the major goals of the presently envisioned experimental program are identified. Results from a recent series of experiments are summarized and the future prospects of this program are discussed.

CONTENTS

1. INTRODUCTION

During the past quarter century, the standard electroweak theory has been established with phenomenal quantitative success. The seminal experiment in parity-violating electron scattering performed at SLAC in 1976 (1) not only confirmed the Lorentz structure of the neutral weak interaction [along with atomic parity violation experiments (2)] but also introduced a powerful new experimental technique: the measurement of helicity dependence in electron scattering. It was realized in the late 1980s (3–5) that one could now use the neutral weak interaction as a precision probe of nucleon structure that could reveal novel features such as strange antiquark-quark ($\bar{s}s$) effects. This led to the initiation of the SAMPLE experiment at the MIT/Bates Linear Accelerator Center to provide the first measurement of the strange-quark contribution to the proton's magnetic moment. Data from this experiment indicate that the strange magnetism of the nucleon differs significantly from typical predictions of models of nucleon structure. Furthermore, the SAMPLE measurements provide evidence for a sizeable nucleon anapole moment; the substantial magnitude of this parity-violating electromagnetic effect was unanticipated by theorists (6), is poorly understood, and is presently the subject of much additional study. The SAMPLE experiment represents the first in a now very active field of ambitious and challenging experiments at several accelerator laboratories, and we herein review the experimental and theoretical development of this subject. The importance of and historical interest in the $\bar{s}s$ contributions to nucleon structure are briefly reviewed in the next section. The sensitivity of the neutral weak form factors determined in parity-violating electron scattering to the sea quark structure of the nucleons is discussed in Sections 3 and 4. Section 5 treats the role of the axial form factor of the nucleon as measured in parity-violating electron-nucleon elastic scattering, which provides access to higher-order processes such as the anapole form factor and electroweak radiative corrections. Thus, the study of parity-violating electron scattering offers an advantageous method to access this novel aspect of weak nucleon structure and provides a sensitive testing ground for calculations of electroweak corrections beyond leading order in perturbation theory. There are also corresponding advances in the experimental methods employed to study the small parity-violating observables, and the present and future experimental program to explore this subject is reviewed in Section 6.

2. STRANGE QUARKS IN THE NUCLEON

For historical reasons, the role of strange quark-antiquark pairs in nucleon structure had been ignored for many years. Traditional constituent quark models were rather successful in treating the nucleon using only up and down quarks. But it is important to remember that, in this approximation, only the degrees of freedom associated with valence quark quantum numbers are active; the effects of sea quarks are considered to be "frozen" as inert aspects of the effective degrees of freedom. The constituent quarks actually do contain internal structure associated with gluons and sea quarks (such as $\bar{s}s$), so even in these simple models of the nucleon, the contribution of $\bar{s}s$ pairs is potentially significant and therefore interesting. In the following discussion, a variety of evidence for the presence of $\bar{s}s$ pairs in the nucleon is reviewed in order to provide the appropriate perspective for consideration of the $\bar{s}s$ content of the neutral weak form factors, to be discussed in Section 4.

2.1. Deep Inelastic Neutrino Scattering

The most direct method of detecting the presence of quarks in nucleons is to employ deep inelastic lepton scattering. The quark structure of the nucleon is described through the use of structure functions that can be determined by measurements of the deep inelastic scattering cross sections. These structure functions depend on the Bjorken scaling variable x, which is interpreted as the fraction of nucleon momentum carried by the struck quark in the infinite momentum frame. Thus, the nucleon quark structure is expressed in terms of the individual quark structure functions $u(x)$, $d(x)$, $\bar{u}(x)$, $\bar{d}(x)$, $s(x)$, $\bar{s}(x)$, etc. Elucidation of the flavor structure is facilitated by using charged-current neutrino and antineutrino interactions. Neutrinos interact with d and s quarks by raising their charge and producing a negative lepton (e.g., $\nu_\mu + d \to \mu^- + u$ or $\nu_\mu + s \to \mu^- + c$). The charmed quarks produced by the s quarks then decay semileptonically yielding μ^+s, and so one observes $\mu^-\mu^+$ pairs from ν_μ interactions with s quarks. Similarly, antineutrinos will produce $\mu^+\mu^-$ pairs from $\bar{s}$ quarks. In this way, measurements of $s(x)$ and $\bar{s}(x)$ have been performed in deep inelastic neutrino and antineutrino experiments (7). The results, shown in Figure 1, indicate that $s(x)$ and $\bar{s}(x)$ are significant at low $x < 0.1$ and that the s and $\bar{s}$ each carry about 2% of the nucleon momentum.

Although deep inelastic scattering is useful as a direct probe for the presence of quarks, it is not possible at present to connect these observations with the common static properties of the nucleon such as the mass, spin, or magnetic moment. Clearly, experimental determination of $\bar{s}s$ contributions to these quantities would be of great interest in our attempt to understand these basic properties of the nucleon.

2.2. Strangeness and the π-N Sigma Term

The strange-quark contribution to the nucleon mass can be addressed by studying the "sigma term" in pion-nucleon scattering (8, 9). One first obtains the value

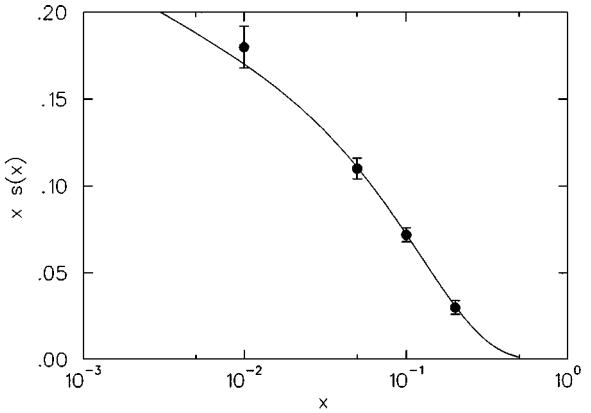

Figure 1 Measured values of $x \cdot s(x)$ at renormalization scale $\mu^2 = 4\ (\mathrm{GeV})^2$ from a next-to-leading order analysis of deep inelastic neutrino scattering (7). There is no significant difference observed between $s(x)$ and $\bar{s}(x)$, so this analysis has assumed they are equal.

of the isospin-even π-N scattering amplitude (from experiment) extrapolated to the pole at squared momentum transfer $q^2 = 2m_\pi^2$ (the Cheng-Dashen point), $\Sigma_{\pi N}$. The most recent analyses (9) indicate that a value of $\Sigma_{\pi N}(2m_\pi^2) \sim 60$ MeV is obtained from the experimental data. This value is then extrapolated (using the theoretical input) to $q^2 = 0$ to give $\Sigma_{\pi N}(0) \sim 45$ MeV. Furthermore, one may utilize hyperon mass relations (assuming the strange quarks contribute linearly in the strange quark mass m_s) to arrive at a prediction for the quantity

$$\sigma \equiv \frac{1}{2M_p}\langle p|\hat{m}(\bar{u}u + \bar{d}d)|p\rangle \simeq 25\,\mathrm{MeV}, \qquad 1.$$

where $\hat{m} \equiv (m_u + m_d)/2$. $SU(3)$ corrections to σ are expected to be about 10 MeV, yielding a predicted value of

$$\sigma_0 \simeq 35\,\mathrm{MeV}. \qquad 2.$$

In the absence of a contribution from $\bar{s}s$ pairs in the nucleon, one would expect $\Sigma_{\pi N}(0) = \sigma_0$. The recent detailed analysis by Gasser et al. (9) examines the various corrections and extrapolations mentioned above. These authors conclude that the difference between $\Sigma_{\pi N}(0)$ and σ_0 implies a finite contribution of $\bar{s}s$ pairs to the nucleon mass

$$m_s\langle p|\bar{s}s|p\rangle \sim 130\,\mathrm{MeV}. \qquad 3.$$

However, one should treat this result with caution for several reasons. There are questions associated with the accuracy of the extrapolation of the π-N amplitudes

into the unphysical region, the precision and consistency of the π-N data, and the effect of $SU(3)$ symmetry breaking in the hyperon mass relations. Indeed, more recent studies (10, 11) of this problem with some input from lattice QCD indicate that the strangeness contribution to the nucleon mass may be about twice as large as that quoted above (10), or nearly zero (11). Further, recent analyses of new experimental work (12, 13) suggest $\Sigma_{\pi N}$ may be significantly larger than previously thought. All of these concerns lead to a reduced confidence in the quoted result, and the uncertainty in the deduced value of the matrix element $\langle p|\bar{s}s|p\rangle$ is probably at the 100% level.

2.3. Strangeness and Nucleon Spin

The flavor structure of the nucleon spin can be addressed by studying spin-dependent deep inelastic lepton scattering. An extensive series of experiments using electron and muon scattering over the past decade have produced an impressive set of data (14). The inclusive scattering of a charged lepton from a nucleon at large momentum transfer can be described by four structure functions: F_1, F_2, g_1, and g_2. Each of these functions depends on the kinematic variables Q^2 (the squared momentum transfer) and the Bjorken scaling variable x. By employing longitudinally polarized incident leptons, one can extract the two spin-dependent structure functions g_1 and g_2 from measurements with the target spin parallel and perpendicular to the incident lepton momentum. Of greatest interest for the present discussion is the leading-order structure function g_1, which contains information directly related to the quark spin structure of the nucleon. The spin-dependent quark structure is described by spin-dependent structure functions $u^+(x)$, $u^-(x)$, $d^+(x)$, $d^-(x)$, $s^+(x)$, and $s^-(x)$, where $+$ (or $-$) refers to the quark spin being parallel (or antiparallel) to the nucleon spin. One usually defines the integrated differences

$$\Delta u \equiv \int_0^1 [u^+(x) - u^-(x)]\, dx \qquad 4.$$

and similarly for Δd and Δs. One can experimentally determine the spin-dependent structure function of the nucleon $g_1(x)$. From these data, one then computes the first moment

$$\Gamma_1 \equiv \int_0^1 g_1(x)\, dx. \qquad 5.$$

For the proton, this quantity is related to Δu, Δd, and Δs by

$$\Gamma_1^p = \frac{1}{2}\left(\frac{4}{9}\Delta u + \frac{1}{9}\Delta d + \frac{1}{9}\Delta s\right). \qquad 6.$$

All of these expressions are modified at finite Q^2 by QCD corrections that introduce a mild but significant Q^2 dependence (15). Similarly, Γ_1^u can be obtained for the neutron.

Having obtained $\Gamma_1^{p,n}$ from experiment, one can combine this information with the isovector axial matrix element [known from neutron beta decay (16)]

$$G_A(Q^2 = 0) = \Delta u - \Delta d = 1.2601 \pm 0.0025 \quad 7.$$

and the octet combination [from hyperon beta decays (17)]

$$a_8 = (\Delta u + \Delta d - 2\Delta s) = -0.60 \pm 0.12 \quad 8.$$

to obtain values for the individual flavor components Δu, Δd, and Δs. The most recent analyses of the experimental results (15) indicate that the fraction of the nucleon spin carried by quark spins is roughly

$$\Delta u + \Delta d + \Delta s = 0.20 \pm 0.10. \quad 9.$$

That is, only 20% of the nucleon's spin is carried by the quark spins.

The actual contribution of strange quarks is more difficult to extract because of its substantial sensitivity to $SU(3)$ breaking effects. However, the recent analyses (14, 15) all tend to favor a result that is in the range

$$\Delta s \simeq -0.1 \pm 0.1. \quad 10.$$

Although this seems rather small, it is quite significant compared with the total spin carried by the quark spins (Equation 10). Nevertheless, concerns associated with $SU(3)$ breaking, the extrapolation of the data to $x = 0$ to form the integrals in Equation 5, and the uncertainties arising from the Q^2 evolution of the structure functions all contribute to reduced confidence in the extraction of Δs using this method.

It has been suggested that the strange spin-dependent structure function $\Delta s(x)$ could be determined in measurements of semi-inclusive kaon production in spin-dependent deep inelastic scattering (18). Although the problem of extrapolation to $x = 0$ would remain, this information would be very helpful in further constraining Δs. Of course, additional uncertainties associated with factorization of the fragmentation process may be encountered in the interpretation of the semi-inclusive asymmetries. The HERMES experiment at DESY will acquire data on this reaction in the near future (19).

It is also possible to obtain information on Δs from elastic neutrino nucleon scattering. As discussed in Sections 3 and 5, the quantity Δs contributes to the neutral axial vector coupling of the nucleon at $Q^2 = 0$. Recent efforts to analyze existing ν_μ-p data (20) indicate that the uncertainties are too large to make a meaningful statement. However, measurements at very low $Q^2 \leq 0.1$ (GeV/c) would be very sensitive to the axial form factor of interest. Such measurements are technically very difficult, but it has been suggested (21) that one should measure the ratio of ν-p to ν-n cross sections in quasielastic scattering from a $Z = N$ nucleus such as carbon. In the $Q^2 = 0$ limit, the ratio for free nucleons is approximately

$$\frac{\sigma_{\nu p}}{\sigma_{\nu n}} \simeq 1 - 2\frac{\Delta s}{G_A}. \quad 11.$$

It has been shown that the nuclear corrections to this ratio in carbon are quite small (21). The feasibility of such a measurement will be investigated in the mini-Boone experiment at Fermilab (R. Tayloe, private communication).

3. PARITY VIOLATION IN ELECTRON SCATTERING: THEORETICAL FORMALISM

The essential aspects of the parity-violating interaction between electrons and other electrically charged objects (generally hadrons composed of quarks, or another electron) can be seen in Figure 2. The dominant amplitude arises from the electromagnetic interaction (photon exchange), whereas the parity-violating neutral weak interaction corresponding to Z boson exchange generates a small amplitude that is detectable via quantum interference. Due to the parity-violating nature of the weak interaction, these interference effects imply the existence of small pseudoscalar observables in electron scattering experiments.

In the standard electroweak model, the Lorentz structure of the neutral weak interaction is a linear combination of vector and axial vector couplings to the Z boson. Aside from the overall normalization governed by the fundamental electric charge e and the Z boson mass M_Z, the electron and the various flavors of quarks have vector and axial vector coupling strengths that depend on the weak mixing angle θ_W, as illustrated in Table 1. The table lists the relative strengths of the couplings (in lowest-order γ- and Z-exchange) of the basic objects of interest in this discussion; the vector interactions are denoted by charges q (q^γ for γ-exchange and q^Z for Z-exchange) and the axial charges are denoted by a^Z.

One very important feature evident in Table 1 is the dependence of the weak vector couplings q^Z on the weak mixing angle θ_W. In the standard electroweak model, this parameter is related (in lowest order) to the neutral (Z) and charged (W) boson masses by the relation

$$\cos\theta_W = \frac{M_W}{M_Z}. \qquad 12.$$

Measurements of the Z and W masses, along with the fine structure constant α and

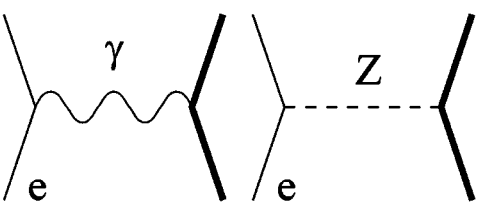

Figure 2 The amplitudes relevant to parity-violating electron scattering. The dominant parity-violating effects arise from the interference of these two amplitudes.

TABLE 1 Electroweak couplings of charged fundamental particles

	q^γ	q^Z	a^Z
e	-1	$-(1-4\sin^2\theta_W)$	$+1$
u	$\frac{2}{3}$	$1-\frac{8}{3}\sin^2\theta_W$	-1
d	$-\frac{1}{3}$	$-1+\frac{4}{3}\sin^2\theta_W$	$+1$
s	$-\frac{1}{3}$	$-1+\frac{4}{3}\sin^2\theta_W$	$+1$

the charged weak coupling constant

$$G_F = \frac{e^2}{4\sqrt{2}M_W^2 \sin^2\theta_W}, \qquad 13.$$

enable a precise determination of the weak mixing angle (16),

$$\sin^2\theta_W = 0.23117 \pm 0.00016. \qquad 14.$$

It should be noted that the value of this constant depends on the renormalization scheme, and we quote the result for the widely utilized modified minimal subtraction (MS) (16) scheme.

The couplings in Table 1 also imply important features of the neutral weak interactions of the composite hadrons comprising everyday matter, protons and neutrons. In experiments at very low energies where nucleons remain intact, the relevant lowest-order elastic couplings to the observed physical particles (electrons and nucleons) are as displayed in Table 2. The separate values for magnetic (μ) and charge (q) interactions are listed and the magnetic moments are in units of $e\hbar/2Mc$, where M is the particle mass. (The magnetic moments μ^γ and weak magnetic moments μ^Z for the nucleons are significantly altered from the Dirac values owing to the internal structure of the nucleons.) The neutral weak vector couplings are evaluated with the value $\sin^2\theta_W = 0.23117$ (16), and the contributions of strange quarks to the neutral weak couplings μ^Z and a^Z are indicated as μ_s and Δs, respectively. The quantities listed in Table 2 are the important couplings relevant for low-energy elastic lepton-nucleon scattering experiments as well as for atomic physics experiments.

TABLE 2 Electroweak couplings of physical particles

	q^γ	μ^γ	q^Z	μ^Z	a^Z
e	-1	-1	-0.074	-0.074	$+1$
p	$+1$	2.79	0.074	$2.08-\mu_s$	$-1.26+\Delta s$
n	0	-1.91	-1	$-2.92-\mu_s$	$+1.26+\Delta s$

In considering parity-violating interactions of electrons one should note that the neutral weak vector coupling of the electron is suppressed because $1-4\sin^2\theta_W \simeq 0.074 \ll 1$. Therefore, the axial vector coupling of the electron is generally dominant in such parity violation experiments.

The axial vector couplings to the light quarks listed in Table 1 imply a definite prediction regarding the isospin behavior of the weak axial interaction of nucleons displayed in Table 2. In the absence of strange quarks, it is evident from Table 1 that the axial coupling is a pure isovector, in which case one would expect the neutral axial vector couplings of the proton and neutron to be exactly equal (except for a sign change). Thus we see that in Table 2 the weak axial coupling to the nucleons is a pure isovector except for the contribution of strange quarks, indicated by the quantity Δs. [This quantity is directly related to sum rules in spin-dependent deep inelastic electron (or muon) scattering discussed in Section 2.3 above.] Any finite signal associated with an isoscalar axial coupling to the nucleons must (in lowest order) be associated with the presence of strange quarks. For the case of parity-violating observables in electron-nucleon interactions, the contribution of the nucleon's axial current is multiplied by the electron's weak charge $q^Z = -(1-4\sin^2\theta_W)$ and is therefore suppressed. (However, the axial current of the nucleon is significant in elastic neutrino-nucleon–scattering experiments, as discussed below in more detail.)

The vector couplings to the quarks are also of great utility in the study of the flavor structure of the nucleon. If one ignores the effects of strange quarks, the charge and magnetic interactions for the proton and neutron are essentially reversed for Z exchange relative to γ exchange. (This is due to the structure contained in Table 1 coupled with the fact that $\sin^2\theta_W \simeq 1/4$.) That is, the charge coupling to the proton is small relative to that of the neutron and the roles of the magnetic moments are reversed ($\mu_p^Z \sim 2 \sim -\mu_n$ and $\mu_n^Z \sim -3 \sim -\mu_p$). Also, one can clearly see effects of $\bar{s}s$ pairs in the vector nucleon couplings, particularly the magnetic moments. Although the absence of a net strangeness in the nucleon implies that the $\bar{s}s$ pairs contribute zero net electric charge (i.e., $q_s = 0$), there is no such prohibition for the magnetic moment and one should expect a contribution μ_s from the strange quarks.

Indeed, the possible contribution of $\bar{s}s$ pairs to the nucleon's magnetism is a subject of substantial current interest and represents the continuation of a long-standing historical tradition of using the magnetic structure of the nucleon as a clue to its internal structure. [We note that in 1933 Frisch & Stern (22) reported the first measurement of the magnetic moment of the proton, the earliest experimental evidence for nucleon substructure.] The neutral weak magnetic moment μ^Z is just as fundamental a property of the nucleon as the usual electromagnetic μ, and it can provide crucial new information on the static magnetic properties of the nucleon. Indeed, as discussed by Kaplan & Manohar (5), the study of neutral weak matrix elements (such as the neutral weak magnetic moment) can be used to determine the $\bar{s}s$ ($\bar{s}s$) matrix elements. Furthermore, as detailed in the following section, one can perform a complete decomposition of these observables into contributions from the three relevant quark flavors (up, down, and strange) (4).

As discussed above, the presence of parity-violating observables in electron scattering experiments is associated (to lowest order) with the interference of γ and Z exchange amplitudes (as indicated in Figure 2). The scattering cross section will generally consist of a helicity-independent piece (dominated by the squared electromagnetic amplitude) and a term that depends on the electron helicity which violates parity (owing to the interference of electromagnetic and neutral weak amplitudes). The parity-violating weak amplitude must contain a product of vector (v^Z) and axial vector (a^Z) couplings. One usually quotes the ratio of helicity-dependent to helicity-independent cross sections, or the parity-violating asymmetry:

$$A = \frac{d\sigma_R - d\sigma_L}{d\sigma_R + d\sigma_L}, \qquad 15.$$

where σ_R and σ_L are the cross sections for right- and left-handed electrons, respectively. This quantity will generally be proportional to a product of neutral weak couplings $v^Z \cdot a^Z$ that contains the physics of interest. Thus, measurement of the helicity dependence in elastic electron-proton scattering can be used to study the neutral weak vector form factors of the nucleon (3, 4).

The parity-violating asymmetry for elastic electron-proton scattering is given by the following expression (23):

$$A = \left[\frac{-G_F Q^2}{4\sqrt{2}\pi\alpha}\right] \frac{\varepsilon G_E^\gamma G_E^Z + \tau G_M^\gamma G_M^Z - (1 - 4\sin^2\theta_W)\varepsilon' G_M^\gamma G_A^e}{\varepsilon\left(G_E^\gamma\right)^2 + \tau (G_M)^2} \qquad 16.$$

$$\equiv -\frac{G_F Q^2}{4\sqrt{2}\pi\alpha} \times \frac{\mathcal{N}}{\mathcal{D}}, \qquad 17.$$

where

$$\tau = \frac{Q^2}{4M_N^2},$$

$$\varepsilon = \frac{1}{1 + 2(1+\tau)\tan^2\frac{\theta}{2}},$$

$$\varepsilon' = \sqrt{\tau(1+\tau)(1-\varepsilon^2)} \qquad 18.$$

are kinematic quantities, $Q^2 > 0$ is the four-momentum transfer, and θ is the laboratory electron scattering angle.

The quantities G_E^γ, G_M^γ, G_E^Z, and G_M^Z are the vector form factors of the nucleon associated with γ- and Z-exchange. As in the case above, the electromagnetic and weak form factors are (in lowest order) related via the flavor dependence of the fundamental couplings in Table 1. The flavor structure of these form factors and the radiative corrections are considered below in Section 4.

The neutral weak N-Z interaction also involves an axial vector coupling G_A^e in the third term of the numerator in Equation 16. The tree-level Z-exchange process is

responsible for the $1 - 4\sin^2\theta_W$ factor that appears in this expression and, as noted in References 6 and 23, higher-order processes can contribute significantly. These include anapole effects and other electroweak radiative corrections as discussed in Sections 5.2 and 5.3.

It will also be useful to consider parity-violating quasielastic scattering from nuclear targets, particularly deuterium. This will provide useful information on the (somewhat uncertain) axial vector form factor contributions. For a nucleus with Z protons and N neutrons, the asymmetry can be written in the simple form (ignoring final-state interactions and other nuclear corrections):

$$A_{\rm nuc} = -\frac{G_F Q^2}{4\sqrt{2}\pi\alpha} \times \frac{N\mathcal{N}_n + Z\mathcal{N}_p}{N\mathcal{D}_n + Z\mathcal{D}_p}, \qquad 19.$$

where $\mathcal{N}_p$ ($\mathcal{N}_n$) is the numerator expression and $\mathcal{D}_p$ ($\mathcal{D}_n$) the denominator (from Equations 17 and 18) for the proton (neutron), respectively.

4. STRANGENESS AND THE NEUTRAL WEAK VECTOR FORM FACTORS

The formalism associated with contributions of strange quark-antiquark pairs to the charge and magnetization distributions of nucleons and nuclei is presented in this section. We begin with a general discussion of the quark flavor structure of the electromagnetic and neutral weak currents of these objects (in lowest order).

The standard electroweak model couplings to the up, down, and strange quarks were listed in Table 1; these imply that the electromagnetic current operator has the simple form

$$\hat{V}_\gamma^\mu = \frac{2}{3}\bar{u}\gamma^\mu u - \frac{1}{3}\bar{d}\gamma^\mu d - \frac{1}{3}\bar{s}\gamma^\mu s. \qquad 20.$$

Also from Table 1, the neutral weak vector current operator is given by an analogous expression,

$$\hat{V}_Z^\mu = \left(1 - \frac{8}{3}\sin^2\theta_W\right)\bar{u}\gamma^\mu u + \left(-1 + \frac{4}{3}\sin^2\theta_W\right)\bar{d}\gamma^\mu d + \left(-1 + \frac{4}{3}\sin^2\theta_W\right)\bar{s}\gamma^\mu s. \qquad 21.$$

Here the coefficents depend on the weak mixing angle. The flavor structure contained in these expressions forms the basis for a program to measure the flavor composition of the vector form factors. The measurements involve matrix elements of these operators (the form factors) which will reflect the underlying flavor dependence of these operators.

4.1. Nucleon Vector Form Factors

The electromagnetic form factors of the nucleon arise from matrix elements of the electromagnetic current operator

$$\left\langle N\left|\hat{V}_\gamma^\mu\right|N\right\rangle \equiv \bar{u}_N\left[F_1^\gamma(q^2)\gamma^\mu + \frac{i}{2M_N}F_2^\gamma(q^2)\sigma^{\mu\nu}q_\nu\right]u_N, \qquad 22.$$

where $F_1^\gamma(q^2)$ and $F_2^\gamma(q^2)$ are the Dirac and Pauli electromagnetic form factors, which are functions of the squared momentum transfer. We also use the Sachs form factors, which are linear combinations of the Dirac and Pauli form factors

$$\begin{aligned} G_E &= F_1 - \tau F_2, \\ G_M &= F_1 + F_2, \end{aligned} \qquad 23.$$

where $\tau \equiv -q^2/4M_N^2 > 0$.

The quark flavor structure of these form factors can be revealed by writing the matrix elements of individual quark currents in terms of form factors:

$$\langle N|\bar{q}^j\gamma^\mu q^j|N\rangle \equiv \bar{u}_N\left[F_1^j(q^2)\gamma^\mu + \frac{i}{2M_N}F_2^j(q^2)\sigma^{\mu\nu}q_\nu\right]u_N, \qquad 24.$$

where $j = u$, d, or s; this defines the form factors F_1^j and F_2^j. Then, using definitions analogous to Equation 24, we can write

$$G_E^\gamma = \frac{2}{3}G_E^u - \frac{1}{3}G_E^d - \frac{1}{3}G_E^s, \qquad 25.$$

$$G_M^\gamma = \frac{2}{3}G_M^u - \frac{1}{3}G_M^d - \frac{1}{3}G_M^s. \qquad 26.$$

In direct analogy to Equation 22, we have expressions for the neutral weak form factors G_E^Z and G_M^Z in terms of the different quark flavor components:

$$\begin{aligned} G_{E,M}^Z = &\left(1 - \frac{8}{3}\sin^2\theta_W\right)G_{E,M}^u + \left(-1 + \frac{4}{3}\sin^2\theta_W\right)G_{E,M}^d \\ &+ \left(-1 + \frac{4}{3}\sin^2\theta_W\right)G_{E,M}^s. \end{aligned} \qquad 27.$$

Again it is important to emphasize that the form factors $G_{E,M}^{u,d,s}$ appearing in this expression are exactly the same as those in the electromagnetic form factors in Equations 26 and 27.

Utilizing isospin symmetry, one then can eliminate the up and down quark contributions to the neutral weak form factors by using the proton and neutron electromagnetic form factors and obtain the expressions

$$G_{E,M}^{Z,p} = (1 - 4\sin^2\theta_W)G_{E,M}^{\gamma,p} - G_{E,M}^{\gamma,n} - G_{E,M}^s. \qquad 28.$$

This is a key result. It shows how the neutral weak form factors are related to the electromagnetic form factors plus a contribution from the strange (electric or magnetic) form factor. Thus measurement of the neutral weak form factor will allow (after combination with the electromagnetic form factors) determination of the strange form factor of interest.

The electromagnetic form factors present in Equations 23 and 24 are very accurately known (1%–2%) for the proton in the momentum transfer region $Q^2 < 1$ (GeV/c)^2. The neutron form factors are not known as accurately as the proton form factors (the electric form factor G_E^n is at present rather poorly constrained by experiment), although considerable work to improve our knowledge of these quantities is in progress. The present lack of knowledge of the neutron form factors will not significantly hinder the interpretation of the neutral weak form factors.

In the derivation of Equation 29, it was assumed that isospin symmetry was exact. Electromagnetic and quark mass effects can cause small violations of isospin symmetry and introduce corrections to this relation. The effects of isospin violation on the extraction of strange form factors from neutral weak and electromagnetic form factors was treated in some detail by Miller (24), who found that these corrections are very small, generally less than about 1% of the electromagnetic form factors, and have only a minor effect on the extraction of the strange form factors.

As mentioned in the previous section, there are electroweak radiative corrections to the coefficients in Equation 29 owing to processes such as those shown in Figure 3. The above expressions for the neutral weak vector form factors $G_{p,n}^Z$ in terms of the electromagnetic form factors $G_{p,n}^\gamma$ are modified according to

$$G_{E,M}^{Z,p} = (1 - 4\sin^2\theta_W)\big(1 + R_V^p\big)G_{E,M}^{\gamma,p} - \big(1 + R_V^n\big)G_{E,M}^{\gamma,n} - G_{E,M}^s. \qquad 29.$$

The correction factors have been computed (6, 23, 25) to be

$$\begin{aligned} R_V^p &= -0.054 \pm 0.033, \\ R_V^n &= -0.0143 \pm 0.0004. \end{aligned} \qquad 30.$$

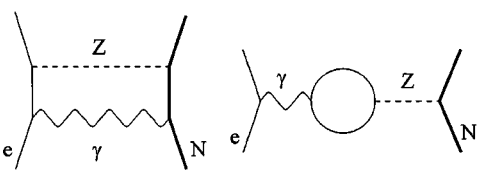

Figure 3 Examples of amplitudes contributing to electroweak radiative corrections ("$\gamma - Z$ box" on the left) and anapole corrections ("$\gamma - Z$ mixing" on the right).

4.2. Strange Magnetism and the Strangeness Radius

The properties of the strange form factors G_E^s and G_M^s near $Q^2 = 0$ are of particular interest in that they represent static properties of the nucleon. Thus, it is customary to define the quantity

$$\mu_s \equiv G_M^s(Q^2 = 0) \qquad 31.$$

as the strange magnetic moment of the nucleon. Since the nucleon has no net strangeness, we find $G_E^s(Q^2 = 0) = 0$. However, one can express the slope of G_E^s at $Q^2 = 0$ in terms of a "strangeness radius" r_s

$$r_s^2 \equiv -6\left[dG_E^s/dQ^2\right]_{Q^2=0}. \qquad 32.$$

4.3. Theoretical Models for the Strange Vector Form Factors

A variety of theoretical methods have been employed in efforts to compute the form factors $G_{E,M}^s(Q^2)$ (or often just the quantities μ_s and r_s). Figure 4 shows two examples of physical processes that may contribute. These are generically known as loop effects and pole effects. The loop effects (26–30) correspond to the fluctuation of the nucleon into a K meson and hyperon. The physical separation of the s and $\bar{s}$ in such processes (or the production of $\bar{s}s$ in a spin singlet) leads to nonzero values of $G_{E,M}^s(Q^2)$. The pole processes (32–34) are associated with the fluctuation of the virtual boson (photon or Z) into a ϕ meson, which is predominantly an $\bar{s}s$ pair. Some attempts have been made to combine the two approaches using dispersion theoretical analyses (35). Other models employ $SU(3)$ extensions of the Skyrme model (36–39) or the Nambu-Jona-Lasinio model (40). Excited hyperons and strange mesons are also included in some treatments, and these contributions seem to be numerically significant (30, 31). A detailed review of the various calculations can be found elsewhere (41).

Table 3 provides a reasonably complete compilation of theoretical results for μ_s and r_s^2. The calculated values of r_s^2 are small and there is no general agreement on the sign. However, there is evidently a trend in Table 3 that one should expect $\mu_s < 0$, generally in the range $-0.8 \rightarrow 0.0$ nuclear magnetons. Notable exceptions

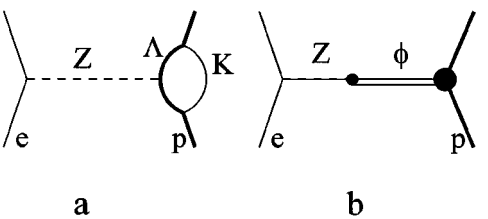

Figure 4 Examples of (*a*) loop and (*b*) pole diagrams used to compute strangeness effects in the nucleon.

TABLE 3 Theoretical predictions for $\mu_s \equiv G_M^s(Q^2 = 0)$ and r_s^2

Type of calculation	μ_s (n.m.)	r_s^2 (fm^2)	Reference
Poles	-0.31 ± 0.09	$0.11 \rightarrow 0.22$	32
Kaon loops	$-0.31 \rightarrow -0.40$	$-0.032 \rightarrow -0.027$	27
Kaon loops	-0.026	-0.01	28
Kaon loops	$\lvert\mu_s\rvert = 0.8$		29
SU(3) Skyrme (broken)	-0.13	-0.10	36
SU(3) Skyrme (symmetric)	-0.33	-0.19	36
SU(3) chiral hyperbag	$+0.42$		37
SU(3) chiral color dielectric	$-0.20 \rightarrow -0.026$	-0.003 ± 0.002	44
SU(3) chiral soliton	-0.45	-0.35	38
Poles	-0.24 ± 0.03	0.19 ± 0.03	33
Kaon loops	$-0.125 \rightarrow -0.146$	$-0.022 \rightarrow -0.019$	30
NJL soliton	$-0.05 \rightarrow +0.25$	$-0.25 \rightarrow -0.15$	40
QCD equalities	-0.75 ± 0.30		45
Loops	$+0.035$	-0.04	31
Dispersion	$-0.10 \rightarrow -0.14$	$0.21 \rightarrow 0.27$	35
Chiral models	$-0.25, -0.09$	0.24	46
Poles	0.003	0.002	34
SU(3) Skyrme (broken)	$+0.36$		39
Lattice (quenched)	-0.36 ± 0.20	$-0.06 \rightarrow -0.16$	42
Lattice (chiral)	-0.16 ± 0.18		43

are References 37 and 39, which analyze the set of baryon magnetic moments in the context of a *SU*(3) generalization of the Skyrme model Hamiltonian.

These model calculations unfortunately have a common difficulty—the need to make important approximations to cover unknown territory. For example, the intuitively attractive picture of a nucleon fluctuating into mesons and other baryons appears to have very large contributions from higher mass states; in a simple (but artificial) limit the contributions cancel. Further, the dispersion calculations have suggested that rescattering is also important and that the simple one-loop fluctuations are again just an approximation and perhaps a rather poor one. Heavy baryon chiral perturbation theory, rather successful in other contexts, suffers generally from the extension to three flavors in that apparently large and, in many cases, unknown counterterms must be included to account for higher-order processes. These difficulties, of course, stem from the fact that experimentally we are separating out a "microscopic" quantity—the $\bar{s}s$ vector currents—which we end up trying to describe with "macroscopic" fields. As is evident from Table 3, the present uncertainties are at the 100% level. There is hope that lattice calculations can help

to sort out these models utilizing effective degrees of freedom by looking at quantities such as those associated with the sea quarks. Indeed, preliminary studies in the quenched approximation have already been performed (42, 43). However, the first two-flavor unquenched calculations are only now producing results and the extension to three flavors is nontrivial. Accurate theoretical description of the strange quark vector currents will therefore be an important topic in hadronic physics for some time to come.

5. AXIAL FORM FACTOR AND THE ANAPOLE MOMENT

As noted in Section 3, the parity-violating interaction of electrons with nucleons involves an axial vector coupling to the nucleon, G_A^e. This term in the parity-violating asymmetry contains several effects beyond the leading-order Z-exchange, which can only be differentiated in theoretical calculations. Nevertheless, it is important to establish that the experimentally observable quantities are well-defined and unambiguous. To this end, we define the neutral weak axial form factors as observed in neutrino scattering, G_A^ν, and the corresponding quantity G_A^e, as indicated in Equation 17. In the following, we discuss the relationship of each of these observables to nucleon beta decay, W- and Z-exchange, and higher-order effects such as the anapole moment.

5.1. Neutron Beta Decay and Elastic Neutrino Scattering

The standard electroweak model relates the axial coupling, G_A, measured in the charge-changing process (such as neutron beta decay) to the neutral process (such as neutrino scattering). For the case of neutrino scattering, the situation is simplified because the neutrino has no (to lowest order) electromagnetic interaction. However, owing to the effect of $\bar{s}s$ pairs in generating the isoscalar neutral weak form factor (see Table 2), in lowest order we have the relation

$$G_A^\nu = G_A\tau_3 + \Delta s. \qquad 33.$$

Δs is the same quantity that appeared in the discussion of spin-dependent deep inelastic scattering in Section 2.3 above. $G_A(Q^2 = 0) = 1.2601 \pm 0.0025$ is determined from neutron beta decay, and the Q^2 dependence is measured in charged-current neutrino scattering to be

$$G_A(Q^2) = \frac{G_A(Q^2 = 0)}{\left(1 + \frac{Q^2}{M_A^2}\right)^2} \qquad 34.$$

with $M_A \simeq 1.05$ GeV. In higher order, G_A^ν also contains contributions from electroweak radiative corrections leading to the modified expression

$$G_A^\nu = G_A\tau_3 + \Delta s + R_\nu \qquad 35.$$

where R_ν represents the radiative corrections, which are of order α.

5.2. Parity-Violating Electron Scattering: Higher-Order Contributions

In parity-violating electron scattering, the neutral weak axial form factor corresponding to tree-level Z-exchange is multiplied by the coefficient $1 - 4\sin^2\theta_W \ll 1$. This suppression of the leading amplitude increases the importance of anapole effects and other electroweak radiative corrections:

$$G_A^e = G_A^Z + \eta F_A + R_e, \qquad 36.$$

where

$$\eta = \frac{8\pi\sqrt{2}\alpha}{1 - 4\sin^2\theta_W} = 3.45, \qquad 37.$$

$G_A^Z = G_A\tau_3 + \Delta s$ (as in Equation 33), F_A is the nucleon anapole form factor (defined below), and R_e are radiative corrections. Typical contributions to R_e and F_A are shown in Figure 3.

As discussed elsewhere (6, 23), the separation of F_A and R_e is actually a theoretical issue and depends on the choice of gauge. In calculations performed to date (M.J. Musolf, unpublished PhD thesis; 25) the anapole type effects associated with the "$\gamma - Z$ mixing" amplitudes are, in fact, the dominant correction. We thus refer to the observable difference between G_A^e and G_A^ν as an anapole contribution, with the caveat that the complete set of radiative corrections must be included in any consistent quantitative theoretical treatment of G_A^e.

The anapole moment has been traditionally defined as the effective parity-violating coupling between real photons and nucleons (47). (In practice, this quantity is observable only at finite momentum transfer associated with the parity-violating interaction between electrons and nucleons.) It appears as an additional term in Equation 23 when one includes the possibility that parity is not strictly conserved (M. J. Musolf, unpublished PhD thesis):

$$\langle N|\hat{V}_\gamma^\mu|N\rangle \equiv -e\bar{u}_N(p')\Big\{F_1\gamma^\mu - \frac{i}{2m}F_2\sigma^{\mu\nu}q_\nu + F_A[G_F(q^2\gamma^\mu - q^\nu\gamma_\nu q^\mu)\gamma^5]\Big\}u(p). \qquad 38.$$

Note that our definition of F_A differs from that used in the atomic physics literature by a factor of m^2G_F with the result that we expect the value of F_A could be of order unity. Thus, F_A could indeed provide a substantial contribution to G_A^e (see Equation 37).

The anapole moment has been considered previously in atomic parity violation experiments. Its definition is analogous to that in Equation 39, except that it is now a form factor of the atomic nucleus (which may involve many nucleons). In that case, the anapole moment is expected to be dominated by many-body weak interaction effects in the nucleus (48). A value for the anapole moment of the cesium atom has recently been reported (49).

Parity-violating electron scattering is not well suited to a determination of Δs, since this contribution is suppressed and the corrections associated with the nucleon axial vector couplings would obscure the interpretation. It may be possible to achieve a better determination of G_A^s in low-energy neutrino scattering, where the axial vector term dominates the cross section and the radiative corrections are under better control. (There is no suppression of the leading Z-exchange amplitude, and diagrams such as those in Figure 3 involving a photon exchange do not contribute to neutrino scattering.)

5.3. Theory of the Anapole Contribution

As mentioned above, aside from the leading Z-exchange term (G_A^Z), the dominant calculated contribution to G_A^e arises from the "$\gamma - Z$ mixing" diagram shown in Figure 3 (M.J. Musolf, unpublished PhD thesis; 25). It should be noted that the evaluation of this amplitude ignores the strong interaction of the nucleon with the quark loop and so may not be numerically accurate. More recently, consideration of additional strong interaction effects associated with mesonic processes have indicated only relatively small additional corrections (50–53). The study of the anapole contributions and other corrections to G_A^e is presently an active area of experimental and theoretical investigation.

6. THE EXPERIMENTAL PROGRAM

6.1. SAMPLE Experiment

The first experiment to determine the weak neutral magnetic form factor of the proton is the SAMPLE experiment at the Bates Linear Accelerator Center. Most of the modern techniques developed for the measurement of small asymmetries in electron scattering experiments are employed in this experiment. Thus, some of the relevant methods are described in detail in this section. Further details are available in the unpublished PhD theses of B. A. Mueller, T. A. Forest, and D. P. Spayde.

The experiment is performed using a 200-MeV polarized electron beam incident on a liquid hydrogen target. The scattered electrons are detected in a large-solid-angle ($\sim$1.5 sr) air Cerenkov detector similar to that in Reference 54 at backward angles $130^\circ < \theta < 170^\circ$. This results in an average $Q^2 \simeq 0.1$ (GeV/c)^2. The expected asymmetry for $G_M^s = 0$ is -7.2×10^{-6} or -7.2 ppm. At these kinematics, the axial term is expected to contribute about 20% of the asymmetry. Figure 5 shows a schematic of the apparatus.

The detector consists of 10 large ellipsoidal mirrors that reflect the Cerenkov light into photomultiplier tubes 8 inches in diameter. Each photomultiplier is shielded from the target and room background by a cast lead shield. The backgrounds involve non-Cerenkov sources of light, which are diagnosed in separate measurements.

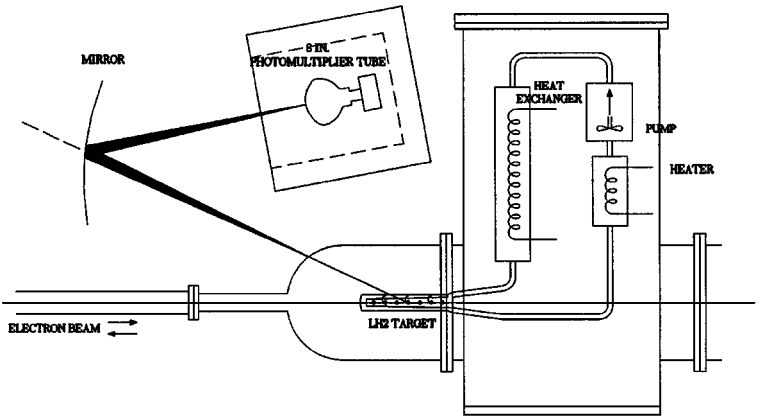

Figure 5 Schematic diagram of the layout of the SAMPLE target and detector system.

Each detector signal is integrated over the $\sim 25\,\mu$s of the beam pulse and digitized. The beam intensity is similarly integrated and digitized. The ratio of integrated detector signal to integrated beam charge is the normalized yield, which is proportional to cross section (plus backgound). The goal is to measure the beam helicity dependence of the cross section, or equivalently, the helicity dependence of the normalized yield. All 10 detectors are combined in software during the data analysis.

The polarized electron source is a bulk GaAs photoemission source, with polarization typically 35%. The laser beam that is incident on the GaAs crystal is circularly polarized by a Pockels cell $\lambda/4$ plate. The helicity is rapidly reversed by changing the voltage on the Pockels cell to reverse the circular polarization of the light. It is possible to manually reverse the beam helicity by inserting a $\lambda/2$ plate, which reverses the helicity of the light relative to all electronic signals. A real parity violation signal will change sign under this "slow reversal." Electronic crosstalk and other effects will not change under slow reversal, so this is an important test to verify that the observed asymmetries are due to real physics rather than spurious systematic effects in the experimental apparatus.

At the backward angles measured in the SAMPLE experiment, the parity-violating asymmetry for elastic scattering on the proton for the incident electron energy of 200 MeV can be written as

$$A_p = \left[\frac{0.026}{\sigma_p}\right]\left[\frac{-G_F Q^2}{\pi\alpha\sqrt{2}}\right]\left[1 - 0.27G_A^e(T=1) - 0.61G_M^s\right]$$
$$= -5.72 + 1.55G_A^e(T=1) + 3.49G_M^s \text{ ppm}. \qquad 39.$$

[The isoscalar component of G_A^e is computed to be very small (50), and we have absorbed it into the leading constant term in these expressions.] The reported

measurement of this asymmetry (55, 56) by the SAMPLE collaboration is

$$A_p = -4.92 \pm 0.61 \pm 0.73\,\text{ppm}. \qquad 40.$$

The analogous expression for quasielastic electron scattering on the deuteron at 200 MeV is

$$\begin{aligned} A_d &= \left[\frac{0.049}{\sigma_d}\right]\left[\frac{-G_F Q^2}{\pi\alpha\sqrt{2}}\right]\left[1 - 0.24G_A^e(T=1) - 0.10G_M^s\right] \\ &= -7.27 + 1.78G_A^e(T=1) + 0.75G_M^s\,\text{ppm}. \end{aligned} \qquad 41.$$

$\sigma_{(p,n)}$ are defined from the electromagnetic cross sections $\sigma_{(p,n)} = \epsilon(G_E^{(p,n)})^2 + \tau(G_M^{(p,n)})^2$, where ϵ and τ are kinematic factors. We have assumed the "static approximation" for the quasielastic scattering from the deuteron, $\sigma_d = \sigma_p + \sigma_n$, as discussed and studied elsewhere (57). Thus we see that the deuteron asymmetry is relatively more sensitive to the contribution from the isovector axial form factor $G_A^e(T=1)$ whereas the proton asymmetry has greater sensitivity to the strange magnetic form factor. Recently, the SAMPLE collaboration has reported a value for this quasielastic deuterium asymmetry (58),

$$A_d = -6.79 \pm 0.64 \pm 0.55\,\text{ppm}. \qquad 42.$$

The expected asymmetry, using the tree-level $G_A^e = G_A^Z$ and $G_M^s = 0$, is $A_d = -9.2$ ppm. Using the calculations of G_A^e in Reference 50 with $G_M^s = 0$, the asymmetry is -8.7 ppm. Thus, the experimental result indicates that the substantial modifications of G_A^e due to anapole effects predicted by Musolf & Holstein (6) are present, but probably with an even larger magnitude than they quoted. It therefore appears that the neutral axial form factor determined in electron scattering is substantially modified from the tree-level Z-exchange amplitude (as determined in elastic ν-p scattering). This is illustrated in Figure 6, which shows the allowed regions for both the proton and deuteron SAMPLE results. This analysis indicates that the magnetic strangeness is small,

$$G_M^s(Q^2 = 0.1) = 0.14 \pm 0.29 \pm 0.31. \qquad 43.$$

We can correct this value for the calculated Q^2 dependence (59) of G_M^s to obtain the following result for the strange magnetic moment:

$$\mu_s = 0.01 \pm 0.29 \pm 0.31 \pm 0.07, \qquad 44.$$

where the third uncertainty accounts for the additional uncertainty associated with the theoretical extrapolation to $Q^2 = 0$.

In addition, assuming the calculated small isoscalar axial corrections are not grossly inaccurate, the isovector axial form factor can be determined from the SAMPLE results to be

$$G_A^e(T=1) = +0.22 \pm 0.45 \pm 0.39, \qquad 45.$$

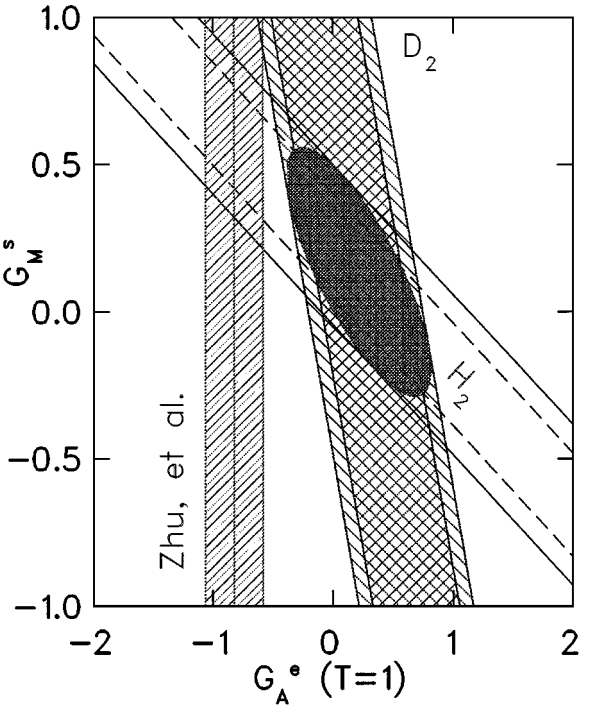

Figure 6 Combined analysis of the data from the two SAMPLE measurements. The two error bands from the hydrogen experiment (55) and the deuterium experiment (58) are indicated. The inner hatched region includes the statistical error and the outer represents the systematic uncertainty added in quadrature. Also plotted is the calculated isovector axial *e-N* form factor $G_A^e\,(T = 1)$ obtained by using the anapole form factor and radiative corrections by Zhu et al. (50).

in contrast to the calculated value (50) $G_A^e(T = 1) = -0.83 \pm 0.26$. This may be an indication that the anapole effects in the nucleon are somewhat larger (by a factor of 2–3) than expected based on these calculations.

6.2. HAPPEX Experiment

The HAPPEX experiment (60, 61) utilized the two spectrometers in Hall A at Jefferson Laboratory to measure parity violation in elastic electron scattering at very forward angles. In this case, the relatively small solid angle of each spectrometer, $\Delta\Omega = 5.5$ msr, was compensated by the very large (0.7 μb/sr) cross section at forward angles ($\theta = 12.3^\circ$), yielding, with a liquid hydrogen target 15 cm long, a rate of roughly 1 MHz in each spectrometer. The scattered electrons were detected by integrating the output of a simple lead-scintillator calorimeter. This calorimeter was shaped to accept only the elastic electrons, which are physically well separated

from the inelastic electrons in the focal plane of the spectrometer. The experiment was performed in two stages. The first used a 100-μA beam with 39% polarization produced from a bulk Ga-As crystal. In the second, a strained Ga-As crystal was used, resulting in a beam polarization of about 70% and a current of 35 μA, slightly improving the overall figure of merit (P^2I).

The measured asymmetry, including the results from both phases of the experiment, is

$$A_p(Q^2 = 0.477\,\mathrm{GeV}^2, \theta_{av} = 12.3^\circ) = -14.60 \pm 0.94 \pm 0.54\,\mathrm{ppm}, \qquad 46.$$

where again the first uncertainty is statistical and the second systematic. The largest sources of systematic uncertainty are measurement of the beam polarization (3.2% of its value) and determination of Q^2 accruing from uncertainty in measurement of the scattering (spectrometer) angle (contributing a 1.8% uncertainty to A_p). The correction for beam-induced false asymmetries amounted to only 0.02 ± 0.02 ppm, or about 0.1% of A_p. There is a significant uncertainty in the result owing to uncertainty in the neutron form factors, as shown in Figure 7 and discussed further below. It should be noted that Figure 7 suggests that the magnitude of the measured asymmetry is less than that with no strange quarks, as is the case for the SAMPLE result.

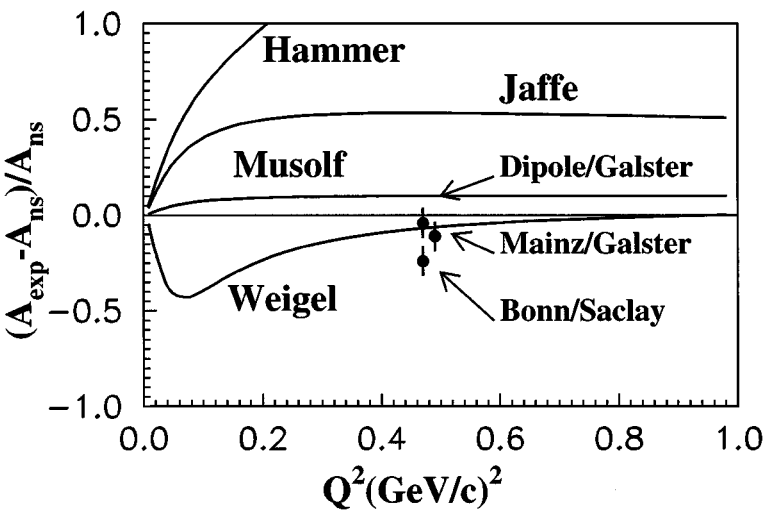

Figure 7 Results from the HAPPEX measurements of parity-violating electron scattering on hydrogen. The three points on the plot correspond to the neutron electromagnetic form factors of (*upper*) G_E^n from Galster (62) and dipole G_M^n; (*middle*) G_E^n from Galster and G_M^n from a Mainz measurement (63); and (*lower*) G_E^n from a Saclay measurement (64) and G_M^n from a Bonn measurement (65). The calculations are from Hammer et al. (33), Jaffe (32), Ramsey-Musolf & Ito (46), and Weigel et al. (40). A_{exp} is the experimentally measured asymmetry and A_{ns} is the predicted asymmetry with no strange quark contribution.

Because the HAPPEX asymmetry was measured at a forward angle, it is in principle sensitive to the three unmeasured form factors—G_E^s, G_M^s, and G_A^e. The axial contribution is relatively small for forward angles (becoming zero at 0°) and is expected to be -0.56 ± 0.23 ppm out of the total of -14.6 ppm, assuming the calculated value (50) for $G_A^e(T=1)$ rather than that measured in the SAMPLE experiment. The other form factors enter in the combination $G_E^s + 0.392 G_M^s$ for these kinematics. The value of this combination, normalized to the most accurately measured proton form factor, G_M^p/μ_p, is

$$\frac{G_E^s + 0.392 G_M^s}{G_M^p/\mu_p} = 0.091 \pm 0.054 \pm 0.039, \qquad 47.$$

where the first uncertainty is a combination of the statistical and systematic uncertainties in the asymmetry combined in quadrature with the above-quoted uncertainty in the axial contribution, and the second is due to the uncertainty in the other electromagnetic form factors (61). The results are particularly sensitive to the neutron magnetic form factor as can be seen in Figure 7; using the results from a different recent G_M^n measurement (65) yields

$$\frac{G_E^s + 0.392 G_M^s}{G_M^p/\mu_p} = 0.146 \pm 0.054 \pm 0.047. \qquad 48.$$

Several experiments are planned for the near future to reduce the uncertainty in G_M^n. Although the results of the HAPPEX experiment exhibit small statistical uncertainties, it is difficult to draw firm conclusions from this single measurement. It appears that there is no strong evidence for the presence of strange quark effects, but the interpretation of these data is hindered by the dependence of the one measured asymmetry on three form factors. At these kinematics, the asymmetry depends on a linear combination of the strange electric and magnetic form factors as well as the neutral axial form factor. At the substantial momentum transfer of these measurements, theory offers little guidance about these form factors or their interrelationships. Therefore, it seems that firm conclusions can only be attempted following further measurements, as discussed below.

6.3. Future Experiments

A number of parity-violating electron scattering experiments are planned for the near future. In order to better understand the contributions of the axial current, the SAMPLE experiment will continue with a second deuterium measurement at a momentum transfer of 0.03 GeV^2 (66). The HAPPEX group is also approved to make a measurement (67) at a momentum transfer of $Q^2 = 0.1$ GeV^2, utilizing new septum magnets placed in front of the existing spectrometers. These septa will allow measurements at more forward angles (roughly 6° scattering angle) in order to increase the cross section at low momentum transfers and hence the overall figure of merit. Other parity-violation measurements performed at Jefferson Laboratory will determine the neutron radius of the Pb nucleus (68) and the asymmetry in

scattering from He at low momentum transfer (69) in order to measure the proton strangeness radius, along with a measurement on He at high momentum transfer (70) ($Q^2 = 0.6$ GeV^2), where early predictions showed a large value of G_E^s. We note that because He is a 0^+, $T = 0$ nucleus, there are contributions neither from G_M nor from G_A, making it particularly advantageous for measurements of G_E^s.

Two new parity violation experiments are being mounted to address the questions of the weak neutral current in the nucleon. The PVA4 experiment (71), under way at the MAMI accelerator in Mainz, will measure both forward and backward asymmetries using an array of PbF_2 calorimeter crystals. The G0 experiment (72), to be performed at Jefferson Laboratory, will use measurements at forward and backward angles to separate the contributions of the charge and the magnetic and axial terms over the full range of momentum transfers from about $Q^2 = 0.1$ to $Q^2 = 1.0$ GeV/c^2.

The PVA4 experiment will initially utilize the 855-MeV beam from the MAMI accelerator to measure the parity-violating elastic scattering asymmetry at an angle centered around 35° ($Q^2 = 0.23$ GeV/c^2). This forward-angle asymmetry will yield the quantity $G_E^s + 0.21 G_M^s$; the measurement began in summer 2000. A 20-μA electron beam with 80% polarization is incident on a 10-cm LH_2 target for the experiment. The detector for the experiment consists of 1022 PbF_2 calorimeter crystals covering a solid angle of 0.7 sr and arranged in a geometry pointing at the target as shown in Figure 8. The first measurements will be made with half the detectors arranged in two diametrically opposed quarters covering half the

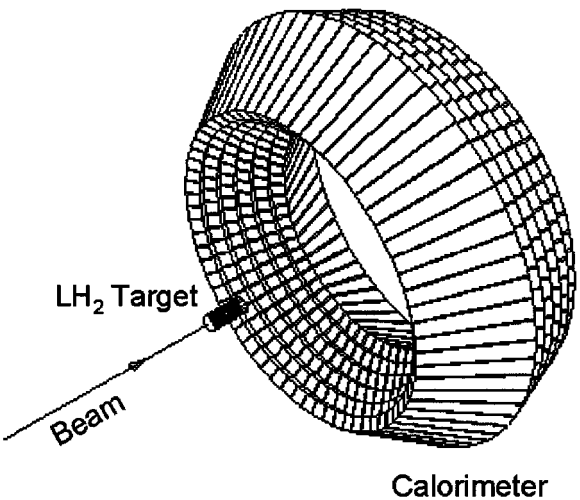

Figure 8 Schematic of the parity-violating electron scattering experiment PVA4 being performed at the Mainz Microtron. The calorimeter consists of an array of 1022 PbF_2 crystals used to count elastically scattered electrons.

total azimuthal angle. The fast Cerenkov signal from the PbF_2 crystals allows separation of elastic and inelastic electrons in hardware. Using an analog sum of signals from a central detector and its eight nearest neighbors, an energy resolution of about 3.5% has been achieved with an integration gate of 20 ns. This allows effective separation of elastic and inelastic electrons—the inelastic yield being about 10 times larger than that from elastic scattering. The same apparatus can be reversed relative to the beam to provide corresponding asymmetries over a range of momentum transfers at backward angles (i.e., with a scattering angle of 145°).

The goal of the G0 experiment is to measure forward proton asymmetries and backward asymmetries for both the proton and deuteron in order to provide a complete set of observables from which the charge currents and the magnetic and axial neutral weak currents of the nucleon can be determined. It will utilize a 40-μA, 70% polarized beam from the Jefferson Laboratory accelerator. The apparatus consists of a superconducting toroidal magnet used to focus particles emerging from a 20-cm liquid hydrogen target to an array of plastic scintillator pairs located outside the magnet cryostat (see Figure 9).

In the first G0 experiment, forward-angle asymmetries will be measured by detecting the recoil protons from elastic scattering. With an acceptance of about 0.9 sr (for scattering angles centered at about 70°), the spectrometer will measure asymmetries over the range $0.12 < Q^2 < 1.0$ GeV^2 with a beam energy of 3 GeV. For this measurement elastic protons are identified by time of flight

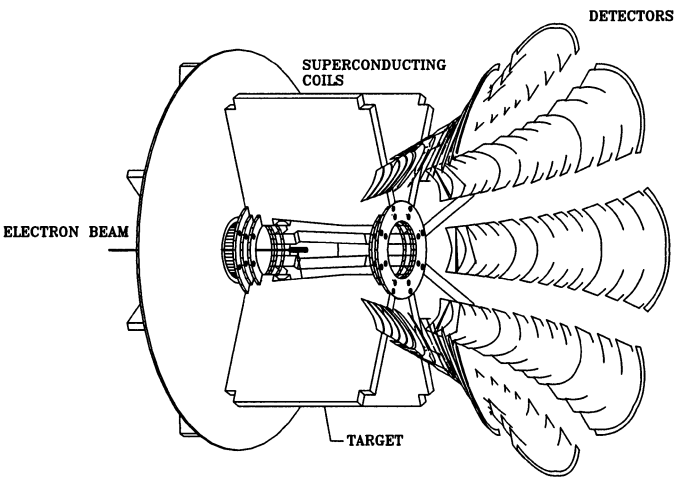

Figure 9 Schematic of the G0 parity-violating electron scattering experiment to be performed at Jefferson Laboratory. A dedicated superconducting toroidal spectrometer will be used to detect recoil protons for forward angle measurements and electrons for backward-angle measurements.

(discriminating against inelastic protons and faster particles such as π^+), and their Q^2 is determined by where in the focal surface they are detected. Background yields and asymmetries are measured concurrently and will be used to correct the elastic asymmetries.

Backward-angle asymmetries will be measured with the same apparatus by reversing its orientation relative to the beam direction. In this case, elastically scattered electrons will be measured at scattering angles around 110°. A set of smaller scintillators will be installed near the exit window of the cryostat to discriminate elastic and inelastic electrons. In combination with the scintillators in the focal surface, this allows a rough measurement of both electron momentum and scattering angle—elastic electrons will appear only in certain well-defined pairs of detectors. Measurements of quasielastic scattering from deuterium at backward angles will require improved particle identification to separate electrons and π^- (essentially absent in the hydrogen measurements). With this capability the G0 experiment will be able to investigate the axial form factor G_A^e over the full range of momentum transfers of the experiment.

7. SUMMARY AND OUTLOOK

The techniques developed to measure parity-violating asymmetries in electron scattering can be utilized to address a variety of interesting and important physics issues, including strange-quark contributions to electroweak form factors and anapole effects.

In the immediate future, there is a program at several laboratories to study the strange quark-antiquark contributions to the vector form factors of the nucleon. Although the presence of strange quarks and antiquarks in the nucleon has been definitively established in deep inelastic neutrino experiments, the role of these $\bar{s}s$ pairs in determining the static properties of the nucleon is still, at present, unclear. Analysis of the π-N sigma term indicates that the $\bar{s}s$ pairs may contribute $\sim$15% to the mass of the nucleon. Future efforts to improve the experimental determination of the π-N amplitudes will be helpful, but it appears that the theoretical uncertainties associated with extracting the sigma term will remain. It therefore appears unlikely that this situation will substantially improve in the near future. The contribution of $\bar{s}s$ pairs to the nucleon spin is also rather uncertain, again because of uncertainties in theoretical interpretation. It appears that the best hope for obtaining better information on Δs lies in low-energy neutrino scattering. However, technical progress in performing these difficult experiments is required before reliable results can be obtained. Nevertheless, this appears to be a promising avenue for development of future experiments and the theoretical interpretation is on rather solid ground.

Parity-violating electron scattering offers a more reliable method for determining the strange quark contributions to the charge and magnetization distributions of the nucleon. In principle, the experiments should yield a detailed mapping of the Q^2 dependence (and therefore the spatial distribution) of the contributions from

all three flavors of quarks in the nucleon. The results of the SAMPLE experiment indicate that at $Q^2 = 0.1$ (GeV/c)^2 the strange magnetic form factor is positive, contrary to most theoretical expectations for μ_s at $Q^2 = 0$. Using recent theoretical estimates for the Q^2 dependence, one obtains a best value of $\mu_s \simeq 0$ from the experiment. Clearly, it is now of great interest to further study G_M^s as a function of momentum transfer. The additional evidence (from the SAMPLE experiment) for a sizeable nucleon anapole moment was also unexpected, and so further measurements to establish this effect and its Q^2 dependence are now essential. The SAMPLE and HAPPEX experiments will continue and several new experiments at other laboratories are planned for the near future. The PVA4 experiment at Mainz, already in progress, will provide a new forward angle asymmetry and possibly other backward-angle asymmetries as well. The G0 experiment will provide a complete separation of G_E^s, G_M^s and G_A^e over a momentum transfer range of 0.1–1.0 GeV^2. Other measurements on ^{4}He and ^{208}Pb will directly determine G_E^s and the radius of the neutron distribution, respectively.

The experimental program of studying parity violation in electron scattering currently offers great potential for providing new and exciting information on fundamental interactions and hadronic structure. The experimental techniques continue to be developed and improved, so we can expect new measurements with unprecedented precision in the future. There is no question that this is a subject with great promise—it only remains to be seen how and when the various new secrets of nature will be revealed by this experimental program.

ACKNOWLEDGMENT

This work was supported by NSF grants PHY-0070182 and PHY-0072044.

LITERATURE CITED

1. Prescott CY, et al. *Phys. Lett.* B77:347 (1978)
2. Bouchiat MA, Bouchiat C. *Rep. Prog. Phys.* 60:1351 (1997)
3. McKeown RD. *Phys. Lett.* B219:140 (1989)
4. Beck DH. *Phys. Rev. D* 39:3248 (1989)
5. Kaplan D, Manohar A. *Nucl. Phys.* B310: 527 (1988)
6. Musolf MJ, Holstein BR. *Phys. Lett.* B242: 461 (1990)
7. Bazarko AO, et al. *Z. Phys. C* 65:189 (1995)
8. Jaffe RL, Korpa CL. *Nucl. Part. Phys.* 17: 163 (1987)
9. Gasser J, Leutwyler H, Sainio ME. *Phys. Lett.* B253:163 (1991)
10. Dong SJ, Lagae JF, Liu KF. *Phys. Rev. D* 54:5496 (1996)
11. Wright SV, Leinweber DB, Thomas AW. *Nucl. Phys.* A680:137 (2000)
12. Olsson M. *Phys. Lett.* B482:50 (2000)
13. Pavan M. nucl-th/9912034
14. Abe K, et al. *Phys. Rev. Lett.* 79:26 (1997); Abe K, et al. *Phys. Rev. Lett.* 75:25 (1995); Abe K, et al. *Phys. Rev. Lett.* 74:346 (1995); Adams D, et al. *Phys. Lett.* B396:338 (1997); Adams D, et al. *Phys. Lett.* B329: 399 (1994); Airapetian A, et al. *Phys. Lett.* B442:484 (1998)

15. Abe K, et al. *Phys. Lett.* B405:180 (1997); Altarelli G, et al. *Nucl. Phys.* B496:337 (1997)
16. Particle Data Group. *Eur. Phys. J.* C54:1 (2000)
17. Jaffe RL, Manohar AV. *Nucl. Phys.* B337: 509 (1990)
18. Close FE, Milner RG. *Phys. Rev. D* 44: 3691 (1991)
19. HERMES Collaboration. Tech. Design Rep. DESY-PRC 93/06 (1993)
20. Garvey GT, Louis WC, White DH. *Phys. Rev.* C48:761–765 (1993)
21. Garvey GT, Krewald S, Kolbe E, Langanke K. *Phys. Lett.* B289:249 (1992); Garvey GT, Kolbe E, Langanke K, Krewald S. *Phys. Rev.* C48:1919 (1993)
22. Frisch R, Stern O. *Z. Phys.* 85:4 (1933)
23. Musolf MJ, et al. *Phys. Rep.* 239:1 (1994)
24. Miller GA. *Phys. Rev. C* 57:1492 (1998)
25. Marciano WJ, Sirlin A. *Phys. Rev. D* 27: 552 (1983); Marciano WJ, Sirlin A. *Phys. Rev. D* 29:75 (1984)
26. Musolf MJ, Burkardt M. *Z. Phys. C* 61:433 (1994)
27. Koepf W, Henley EM, Pollock SJ. *Phys. Lett.* B288:11 (1992)
28. Holstein BR. In *Proc. Caltech Workshop on Parity Violation in Electron Scattering*, ed. EJ Beise, RD McKeown, p. 27. Singapore: World Sci. (1990)
29. Ito H. *Phys. Rev. C* 52:R1750 (1995)
30. Geiger P, Isgur N. *Phys. Rev. D* 55:299 (1997)
31. Hannelius L, Riska D. *Phys. Rev. C* 62: 045204 (2000); Hannelius L, Riska D, Glozman L-Y. *Nucl. Phys.* A665:353 (2000)
32. Jaffe RL. *Phys. Lett.* B229:275 (1989)
33. Hammer HW, Meissner U-G, Drechsel D. *Phys. Lett.* B367:323 (1996)
34. Meissner UG, et al. hep-ph/9701296
35. Musolf MJ, Hammer H-W, Drechsel D. *Phys. Rev. D* 55:2741 (1997)
36. Park NW, Schechter J, Weigel H. *Phys. Rev. D* 43:869 (1991)
37. Hong S, Park B. *Nucl. Phys.* A561:525 (1993)
38. Christov CV, et al. *Prog. Part. Nucl. Phys.* 37:1 (1996)
39. Hong S-T, Park B-Y, Min D-P. nucl-th/ 9706008
40. Weigel H, et al. *Phys. Lett.* B353:20 (1995)
41. Beck DH, Holstein BR. *Int. J. Mod. Phys. E.* In press. hep-ph0102053
42. Leinweber DB, Thomas AW. *Phys. Rev. D* 62:074505 (2000)
43. Dong SJ, Liu KF, Williams AG. *Phys. Rev. D* 58:074504 (1998)
44. Phatak SC, Sahu S. *Phys. Lett. B* 321:11 (1994)
45. Leinweber D. *Phys. Rev. D* 53:5115 (1996)
46. Ramsey-Musolf MJ, Ito H. *Phys. Rev. C* 55:3066 (1997)
47. Zel'dovich I. *JETP Lett.* 33:1531 (1957)
48. Haxton WC, Henley EM, Musolf MJ. *Phys. Rev. Lett.* 63:949 (1989); Haxton W. *Science* 275:1753 (1997)
49. Wood CS, et al. *Science* 275:1759 (1997)
50. Zhu S-L, et al. *Phys. Rev. D* 62:033008 (2000)
51. Riska DO. *Nucl. Phys.* A678:79 (2000)
52. Maekawa CM, van Kolck U. *Phys. Lett.* B478:73 (2000)
53. Maekawa CM, Viega JS, van Kolck U. *Phys. Lett.* B488:167 (2000)
54. Heil W, et al. *Nucl. Phys.* B327:1 (1989)
55. Spayde DT, et al. *Phys. Rev. Lett.* 84:1106 (2000)
56. Mueller BA, et al. *Phys. Rev. Lett.* 78:3824 (1997)
57. Hadjimichael E, Poulis GI, Donnelly TW. *Phys. Rev. C* 45:2666 (1992)
58. Hasty R, et al. *Science* 290:2117 (2000)
59. Hemmert TR, Meissner U-G, Steininger S. *Phys. Lett.* B437:184 (1998)
60. Aniol KA, et al. (HAPPEX Collaboration). *Phys. Rev. Lett.* 82:1096 (1999)
61. Aniol KA, et al. (HAPPEX Collaboration). nucl-ex/00060002
62. Galster S, et al. *Nucl. Phys.* B32:221 (1971)
63. Anklin H, et al. *Phys. Lett.* B428:248 (1998)
64. Platchkov S, et al. *Nucl. Phys.* A510:740 (1990)

65. Bruins EEW, et al. *Phys. Rev. Lett.* 75:21 (1995). These data were corrected downward by 25% of the difference with Ref. 63 by the authors of Ref. 61, based on a private communication with B. Schoch
66. Ito T, spokesperson. MIT-Bates Lab experiment 00:04 (2000)
67. Kumar K, Lhuillier D, spokespersons. Jefferson Lab experiment 99-115 (1999)
68. Michaels R, Souder P, Urciuoli R, spokespersons. Jefferson Lab experiment 00-003 (2000)
69. Armstrong D, spokesperson. Jefferson Lab experiment 00-114 (2000)
70. Beise E, spokesperson. Jefferson Lab experiment 91-004 (1991)
71. von Harrach D, spokesperson; Maas F, contact person. Mainz experiment PVA4 (1993)
72. Beck D, spokesperson. Jefferson Lab experiment 00-006 (2000)

Annual Review of Nuclear and Particle Science
Volume 51, 2001

CONTENTS